Scaling of repeating earthquakes at the transition from aseismic to seismic slip

Olivier Lengliné[1], Jean-Paul Ampuero[2], and Jean Schmittbuhl[3]

[1]Université de Strasbourg, IPGS, CNRS
[2]Institut de Recherche pour le Développement
[3]CNRS/Université de Strasbourg

November 24, 2022

Abstract

Some observations of repeating earthquakes show an unusual, non self-similar scaling between seismic moment and corner frequency, a source property related to rupture size. These observations have been mostly reported in regions at the transition from stable to unstable slip, in geothermal reservoirs and subduction zones. What controls the non self-similarity of these ruptures and how this is linked to the frictional stability of the interface are still open questions. Here we develop seismic cycle simulations of a single unstable slipping patch to investigate the mechanics underlying this behavior. We show that temporal changes of normal stress on a fault can produce ruptures that exhibit the observed anomalous scaling. Our results highlight the role of fault zone fluid pressure in modulating the effective normal stress and contributing to the sliding stability of the fault.

Scaling of repeating earthquakes at the transition from aseismic to seismic slip

O. Lengliné[1], J.P. Ampuero[2], J. Schmittbuhl[1]

[1]EOST/ITES, Université de Strasbourg/CNRS, UMR 7063, 5 rue René Descartes, 67084 Strasbourg Cedex, France
[2]Université Côte d'Azur, IRD, CNRS, Observatoire de la Côte d'Azur, Géoazur, 250 rue Albert Einstein, Sophia Antipolis, 06560 Valbonne, France

Key Points:

- Effective normal stress influences the properties of repeating earthquakes in a rate-and-state friction model
- Fluctuations of effective normal stress reproduce the unusual scaling between moment and rupture size of repeating earthquakes
- Non self-similar scaling is an indicator of proximity to the transition between seismic and aseismic slip

Corresponding author: Olivier Lengliné, `lengline@unistra.fr`

Abstract

Some observations of repeating earthquakes show an unusual, non self-similar scaling between seismic moment and corner frequency, a source property related to rupture size. These observations have been mostly reported in regions at the transition from stable to unstable slip, in geothermal reservoirs and subduction zones. What controls the non self-similarity of these ruptures and how this is linked to the frictional stability of the interface are still open questions. Here we develop seismic cycle simulations of a single unstable slipping patch to investigate the mechanics underlying this behavior. We show that temporal changes of normal stress on a fault can produce ruptures that exhibit the observed anomalous scaling. Our results highlight the role of fault zone fluid pressure in modulating the effective normal stress and contributing to the sliding stability of the fault.

Plain Language Summary

The observation that some earthquakes have nearly similar source lengths but varying magnitude is at odds with empirical earthquake scaling relations observed worldwide. Here we test how the influence of fluid pressure (or, equivalently, effective normal stress) on the fault could explain this atypical observation. We run numerical simulations of a fault containing an asperity that can produce repeating earthquakes. We observe that this asperity can slip seismically or seismically depending on the value of the effective normal stress imposed on the fault. For a given asperity size, there exists a range of effective normal stress that leads to earthquakes with quasi identical lengths but strongly varying magnitude. The relation between these two quantities is close to the one observed for these atypical earthquakes on natural faults. We thus propose that an explanation for this anomalous scaling can be related to the fluctuations of fluid pressure within a fault.

1 Introduction

The increase of pore-pressure in fault zones has been linked in many instances to the occurrence of earthquakes (e.g. Miller, 2013; Lengliné et al., 2017). This is mainly explained by the resulting decrease of effective normal stress bringing the fault closer to frictional failure (Gischig, 2015). Slip on faults that reach failure is then responsible for induced earthquakes. However, the onset of slip does not imply slip is unstable: it could be aseismic or seismic, i.e. having low or high rupture speed, respectively, compared to seismic wave speeds. Indeed, in numerous instances the increase of pore pressure in seismogenic faults has been suggested to promote aseismic slip, such as in geothermal reservoirs (e.g. Cornet et al., 1997), in controlled experiments at various scales (Passelègue et al., 2020; De Barros et al., 2018), in crustal rift zones (De Barros et al., 2020) or in subduction interfaces (Warren-Smith et al., 2019). Induced aseismic slip often goes along with repeating seismic signals interpreted as radiated by the rupture of seismic patches embedded in an otherwise creeping fault. Such repeating signals have been observed in various contexts, including geothermal reservoirs (e.g. Bourouis & Bernard, 2007) or subduction zones, where they take the form of low frequency earthquakes (e.g. Frank et al., 2015). The analysis of these repeating earthquakes has revealed an intriguing behavior: the relation between their corner frequency, f_c (generally interpreted in terms of characteristic rupture length, l), and their seismic moment, M_0, does not follow the typical scaling law (Harrington & Brodsky, 2009; Bouchon et al., 2011; Lengliné et al., 2014; Bostock et al., 2015; Lin et al., 2016; Farge et al., 2020; Cauchie et al., 2020). Indeed, in these examples it was observed that the moment can span nearly 2 orders of magnitude while the rupture length varies only weakly. This is at odds with the scaling $M_0 \propto \Delta\sigma l^3$, where $\Delta\sigma$ is the stress drop, inferred for most earthquakes worldwide and classically associated to self-similar rupture models (e.g. Duputel et al., 2013). However, this equation also shows that a repeating earthquake sequence that satisfies the self-similar scaling with almost constant l but variable $\Delta\sigma$ could explain the atypical observation qualitatively. Changing $\Delta\sigma$ by changing fluid pressure is an obvious such scenario, which we consider here. We further use a numerical modeling approach to reproduce quantitative aspects of the anomalous source scaling observations. In particular, we investigate how a pore pressure perturbation on a fault can modify the nucleation of micro-earthquakes and the proportion of aseismic slip. We analyze the variations of the source parameters of the simulated seismic events as a function of the effective normal stress perturbation. We find that the abnormal scaling relation can emerge from such a scenario and is quantitatively explained by the model.

2 Model

2.1 A rate-and-state friction model

In earthquake cycle models, the equations governing slip on a fault are often modeled assuming rate-and-state state friction (Dieterich, 1992). We follow that framework and describe the modeling equations in Supplementary S1. Under this model assumption, the stability of slip is governed by the balance between the shear stress imposed on the fault and the frictional strength. In a 1D spring slider model, unstable slip occurs when the rigidity of the medium, k, is higher than a critical rigidity (Scholz, 1998),

$$k^* = \frac{(b-a)\sigma_n^{\text{eff}}}{D_c}, \tag{1}$$

where a and b are rate-and-state friction parameters that control the response of the friction coefficient to a change of slip velocity and of fault state variable, respectively, D_c is a characteristic slip distance for the evolution of the state variable, and $\sigma_n^{eff} = \sigma_n - P_p$ is the effective normal stress on the fault. No spontaneous instability occurs if $(b-a) < 0$, i.e. if the fault is velocity-strengthening at steady state. If σ_n^{eff} decreases then k^* decreases and the fault is less prone to unstable sliding. The rigidity of a locked circular patch of radius L on a plane driven by a remote stress is

$$k = \frac{G}{2L} \tag{2}$$

where G is the shear modulus of the elastic medium (Ampuero & Rubin, 2008). Combining equations (1) and (2) gives the minimum size of the circular patch for nucleation of an instability

$$L_c = \frac{D_c G}{2(b-a)\sigma_n^{\text{eff}}}. \tag{3}$$

A decrease of the effective normal stress causes an increase of L_c. Thus, increasing the pore-pressure on a fault may stabilize its seismogenic patches and turn them into aseismic patches. It may also lead to an intermediate behavior in which seismogenic patches become subdued seismic patches, producing earthquakes with smaller moment compared to their unperturbed pore-pressure state. Here we investigate these intermediate cases with the help of a numerical model.

2.2 Modeling the fault

We consider a quasi-dynamic numerical model of a fault governed by rate-and-state friction (Luo et al., 2017; Luo & Ampuero, 2018), as described in Supplementary Text S1. We investigate a simple model of 1D straight fault embedded in a 2D elastic medium, driven by a far field loading and slipping in the anti-plane direction. While there might be quantitative differences between quasi-dynamic and fully-dynamic models (Thomas et al., 2014), we consider that the dynamic stress changes carried by seismic waves will not modify the results obtained here because we focus on isolated asperities with simple geometry. Moreover, we are mostly interested in the variation of observed parameters rather than on their absolute values, such that our approximate representation of co-seismic stress transfer should not impact the observed relative trends. We consider an asperity described as a potentially unstable patch with $a < b$. The rate-and-state friction properties a, b and D_c are assumed constant and independent on pore-pressure. While such a dependency is possible, as reported in (Scuderi & Collettini, 2016), we hypothesize that its effect is small compared to that of the effective normal stress change, and thus does not qualitatively affect the interpretation of our results.

We adopt similar properties of the fault and of the nucleation patch as (Chen & Lapusta, 2009) except that we consider a 1D fault. The elastic medium has a shear modulus $G = 30$ GPa and the far field loading velocity is $V_l = 10^{-9}$ m/s. The fault has a steady state friction coefficient $\mu_{ss} = 0.6$ at the sliding velocity of $V_{ss} = V_l$. A velocity-weakening patch of length L lies at the middle of the fault with $a = 0.015$ and $b = 0.019$. Outside this patch we consider a velocity strengthening zone with $a = 0.019$ and $b = 0.015$. The total modeled domain has a length of $L_x = 1000$ m and outside the domain we impose stable sliding at the plate velocity. The critical slip distance, D_c, is set to 160 μm.

We do the simulations with the boundary element software QDYN (Luo et al., 2017). The fault is decomposed into $N = 1024$ elements. The element size, $dx = L_x/N$, is between 3 and 16 times smaller than the process zone size $L_b = GD_c/b\sigma_{eff}$ for the range of values of σ_{eff} we considered, ensuring that the numerical model has proper spatial resolution. To avoid the influence of the initial conditions, we only considered the results after several earthquake cycles have occurred. Each simulation is performed under temporally constant and spatially uniform normal stress. We systematically study the influence of the normal stress on the sliding stability of seismic fault patches of different sizes L.

3 Results

We first consider a velocity weakening region of half-size $R = L/2 = 100$ m. We run several simulations by imposing various values of the effective normal stress (typically between 20 and 100 MPa). We show in supplementary material (Text S2, Figure S2 and Tables S1 and S2) that the alternative approach of applying a step in σ_n at some time within a repeating earthquake cycle leads to similar results as those presented here. Under constant normal stress and constant remote loading rate, the velocity-weakening patch may experience phases of slip acceleration (instabilities). We track the evolution of the maximum slip velocity in Figure 1. It remains close to the loading velocity most of the time, punctuated by transient increases of slip rate. These transients only occur for a sufficiently large normal stress. Below this normal stress threshold, the simulated fault is stable and no instability developed. We define $v_{th} = 1$ cm/s as the velocity threshold separating aseismic from seismic slip, as in previous studies (e.g Chen & Lapusta, 2009). When the normal stress is too low the slip rate remains lower than v_{th}; we then consider that all the slip on the asperity, even during the slip event, is aseismic. We observe that the maximum slip speed increases with increasing normal stress and exceeds v_{th} when σ_n becomes larger than about 30 MPa. The results of Rubin and Ampuero (2005) suggest that, for an antiplane rupture, the minimum normal stress required to cause seismic slip on a velocity-weakening patch of half-size R is

$$\sigma_n = \frac{2GbD_c}{\pi(b-a)^2 R}, \qquad (4)$$

Given our parameters values, we have $\sigma_n = 36$ MPa, close to the observed value. For higher values of normal stress, the maximum slip velocity remains around 1 m/s. Therefore, there exists a minimum normal stress value above which seismically detectable events exist (Figure 1). Such prediction is a well known behavior of the rate-and-state friction

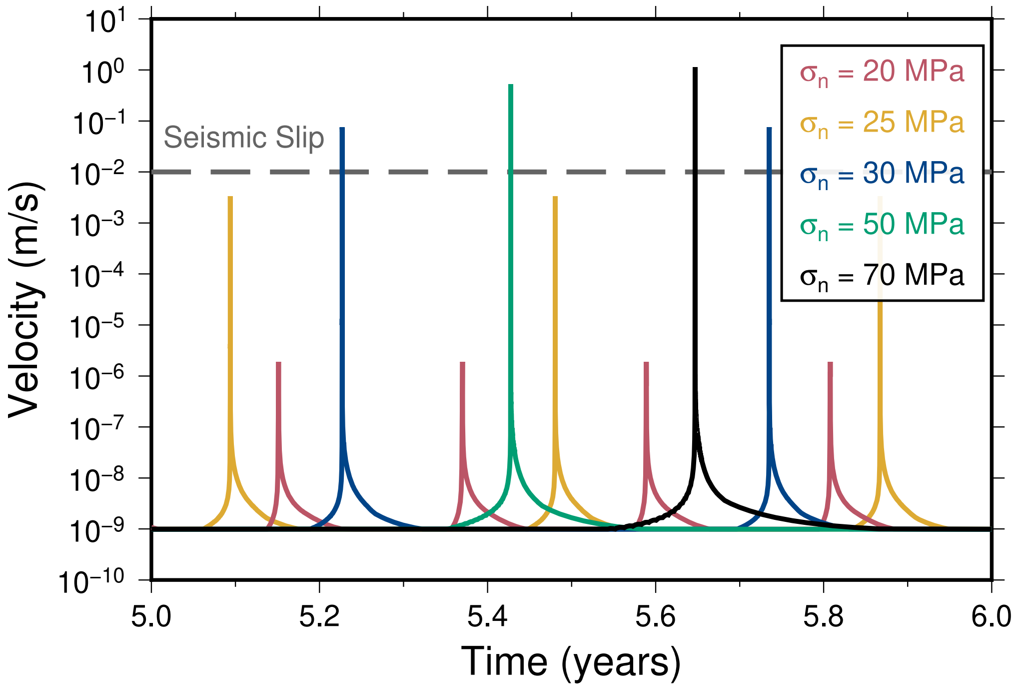

Figure 1. Examples of maximum slip rate evolution for a fault model of length L_x= 1000m, an asperity of half-size R = 100 m driven by a constant loading rate, V_l= 10^{-9} m.s^{-1}. Each curve results from a different simulation with a different normal stress (see legend). The gray dashed line indicates the threshold slip rate, v_{th}, used here to define seismic slip.

model, in which the slip behavior of an isolated asperity is controlled by the ratio between the nucleation length defined by (Rubin & Ampuero, 2005) and the patch length (Rubin, 2008; Barbot, 2019).

We now document how the seismic moment evolves when the normal stress changes during seismic cycles. We determine the starting time, t_s, and ending time, t_e, of each seismic event as the times when the maximum slip rate becomes larger than and lower than v_{th}, respectively. For each event, we compute the distribution of co-seismic slip, D, as a function of the distance to the center of the asperity, x_i, as

$$D(x_i) = \sum_{\substack{t=t_s \\ v(t,x_i)>v_{th}}}^{t_f} u(x_i, t) \tag{5}$$

where $u(x_i, t)$ and $v(x_i, t)$ are respectively the slip and the slip rate computed along the fault at position x_i and at time t (see Figure 2). The position x_i varies from $-L_x/2$ to $L_x/2$ in N steps dx. We convert this distribution of slip from an 1D fault to slip on a (2D) fault plane following the approach of (Lapusta & Rice, 2003; Rubin & Ampuero, 2005) which assumes a radial symmetry of the slip profile, centered at the middle of the asperity, such that the seismic potency, P_0, is computed as

$$P_0 = 2\pi \sum_{x_i=0}^{L_x/2} D(x_i) x_i dx. \tag{6}$$

Finally, the seismic moment is obtained from $M_0 = GP_0$.

We report in Figure 3 the evolution of the seismic moment, M_0 as a function of the effective normal stress, σ_n. From the aseismic/seismic transition up to the maximum achieved seismic moment, M_0 increases by 2 orders of magnitude. Thus the same asperity can produce earthquakes with various seismic moments depending on its normal stress. We also report on the same figure the rupture size of seismic events, r. We simply consider that $r = \max(x) \mid v(x,t) > v_{th}\,, t \in [t_s; t_e]$. We observe that r grows monotonically with the effective normal stress. The values of r are distributed around the values of the half-size of the unstable patch, R, and typically vary over a range of $\pm$ 20 %.

To document how this observation translates in the moment versus radius scaling of earthquakes, we run simulations with different asperity radius ($R = L/2 = 30$, 70, 100 and 300 m) and, for each simulation, we extract the seismic moment and rupture size of each event when varying the normal stress. For simulations performed with $R =$ 300 m we increased the total modeled domain to a length of 2000 m and the number of elements to 2048. We show in Figure 4 the scaling of moment versus rupture size. We observe that, globally, all results fall within the typical scaling

$$M_0 = \frac{7}{16}\Delta\sigma r^3 \tag{7}$$

where $\Delta\sigma$ is the stress drop of a circular crack model (Eshelby, 1957). The range of stress drops identified from Figure 4 varies over 2 orders of magnitude, between 1 and 100 MPa. The lowest stress drops are observed for the lowest values of the normal stress and, as the normal stress increases, so does the stress drop, as previously observed by Kato (2012). As expected from equation 4, for a given asperity size, R, a seismic rupture is only observed for a sufficiently high normal stress. Below this value, the rupture is entirely aseismic (based on our definition). We note that the smaller size earthquakes need only a slight decrease of normal stress to undergo a profound variation of stress drop, while for larger ruptures the change of normal stress required to produce the same effect is more important. This suggests that the effect of normal stress is mainly visible on the smaller ruptures.

For a given seismic patch or asperity size, the scaling between moment and rupture size appears to depart from equation 7, showing a sharp increase of moment with rupture size. We document this scaling of the moment with rupture size within a seismic patch (i.e. a repeating earthquake sequence corresponding to a set of events with a similar asperity size but various prescribed values of normal stress). To reveal this connection, we compute for each of the four seismic patch sizes, R, the normalized moment, $M_0/\langle M_0\rangle$, and the normalized rupture size, $r/\langle r\rangle$, normalizing by their mean values. Despite some scatter, the two orders of magnitude variation of the normalized moment is retrieved while the variation of the normalized rupture size is small (Figure 5). These results clearly indicate that, for repeating ruptures on a seismic patch with varying normal stress, a moment - size scaling emerges with an exponent much higher than the value of 3 expected from self-similarity. A linear least squares regression between the logarithm of the normalized moment and the logarithm of the normalized rupture size reveals that the two quantities are well related by a linear relation with a slope of 12 (Figure 5). We acknowledge however that a power law model is of limited quality due to the very small range of normalized rupture size and one could also consider other forms of laws to fit this data. However, we assume this power-law expression as it is the one used in natural cases.

4 Discussion

Our results can be compared to observations from active faults. For example, Bostock et al. (2015) resolve a similar scaling as in Figure (5) linking the corner frequency to the moment of low frequency earthquakes in the Cascadia subduction zone. Assuming the corner frequency is inversely proportional to the rupture length, as in classical earthquake source models (Savage, 1972), the moment - size exponent for the low frequency earthquakes in Cascadia is around 10. Similarly, Farge et al. (2020) resolve such an anoma-

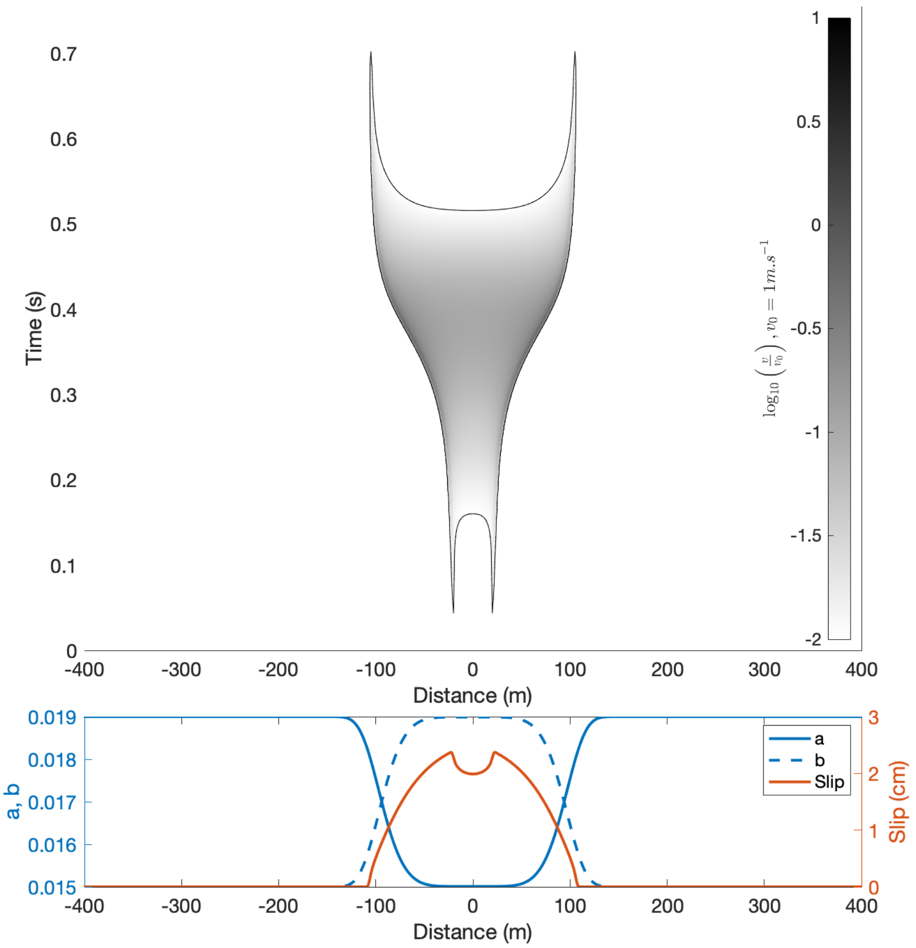

Figure 2. Top: Slip rate as a function of time, t and distance along fault, x during a simulated earthquake (grayshade). Only slip rate higher than v_{th}, indicating a seismic rupture are shown and highlighted with the black contour interval. The time is set here such that t_s=0. The simulation is performed for R=100m and σ_n = 50 MPa (Slip contours for other normal stresses are represented in Figure S1). Bottom: Values of the a and b parameters of the friction law along the fault (blue plain and dashed lines). The seismic slip profile, $D(x)$ computed for this rupture is shown in orange. We extract the length of the seismic rupture from this profile as the maximum position along the fault where $D(x)$ is non-zero which in this example is around 106m.

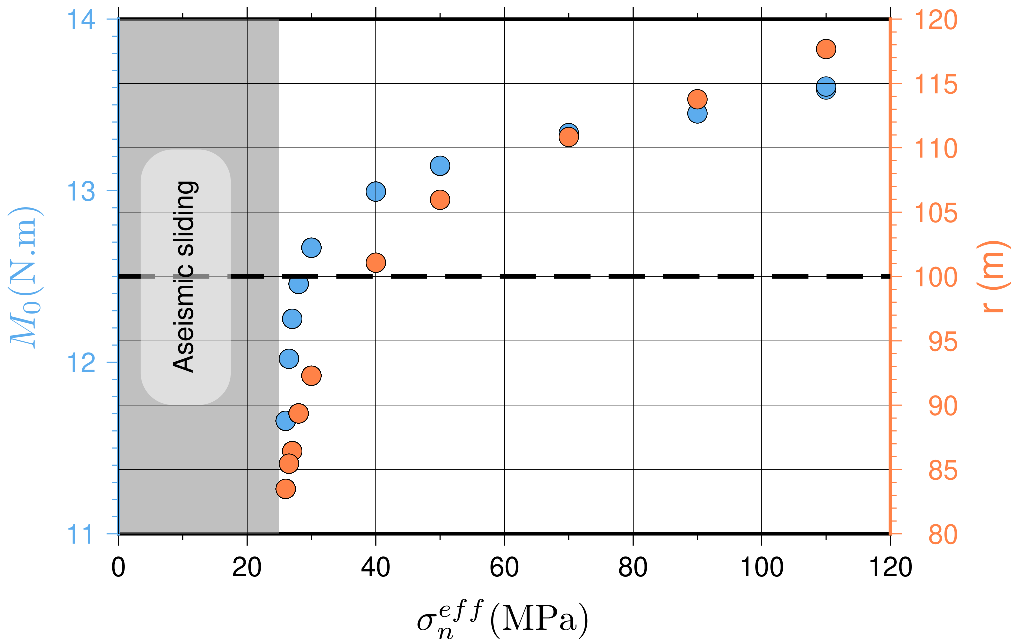

Figure 3. Variation of the moment, M_0 (blue circles) and the rupture length, r (red circles) for simulation of a seismic patch with R=100m (denoted by a black dashed line) as a function of the effective normal stress. For a too low normal stress, typically just below 30 MPa, no seismic rupture is observed and the entire slip is aseismic.

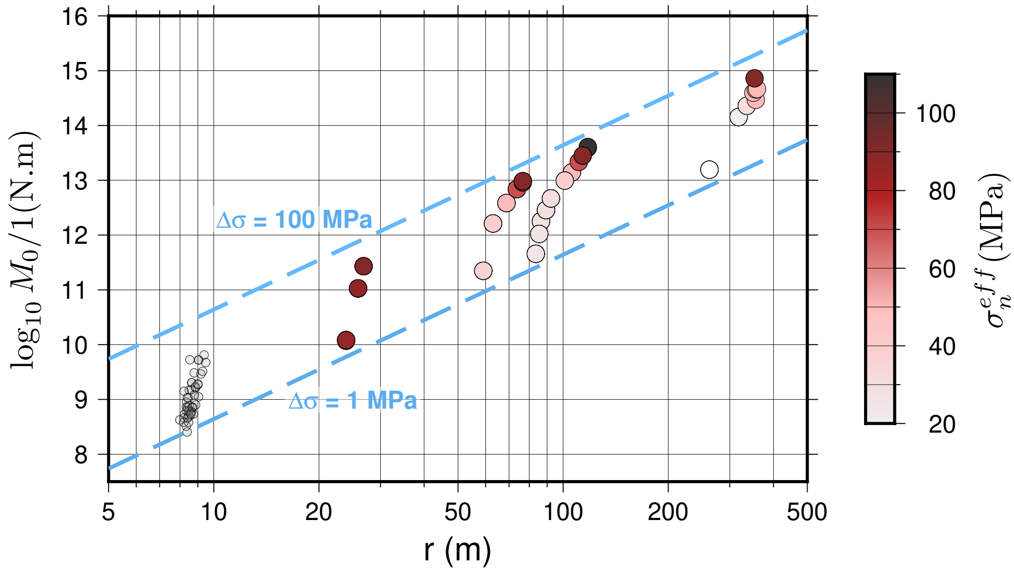

Figure 4. Moment, M_0 as a function of the rupture size, r computed for four different sizes of asperity, R (colored circles). The color of each circle refers to the normal stress used during each simulation. The dashed blue lines indicate the scaling $M_0 \propto r^3$ considering a stress drop of 1 or 100 MPa. The gray transparent dots show for comparison the scaling of a repeating earthquake sequence identified in (Cauchie et al., 2020).

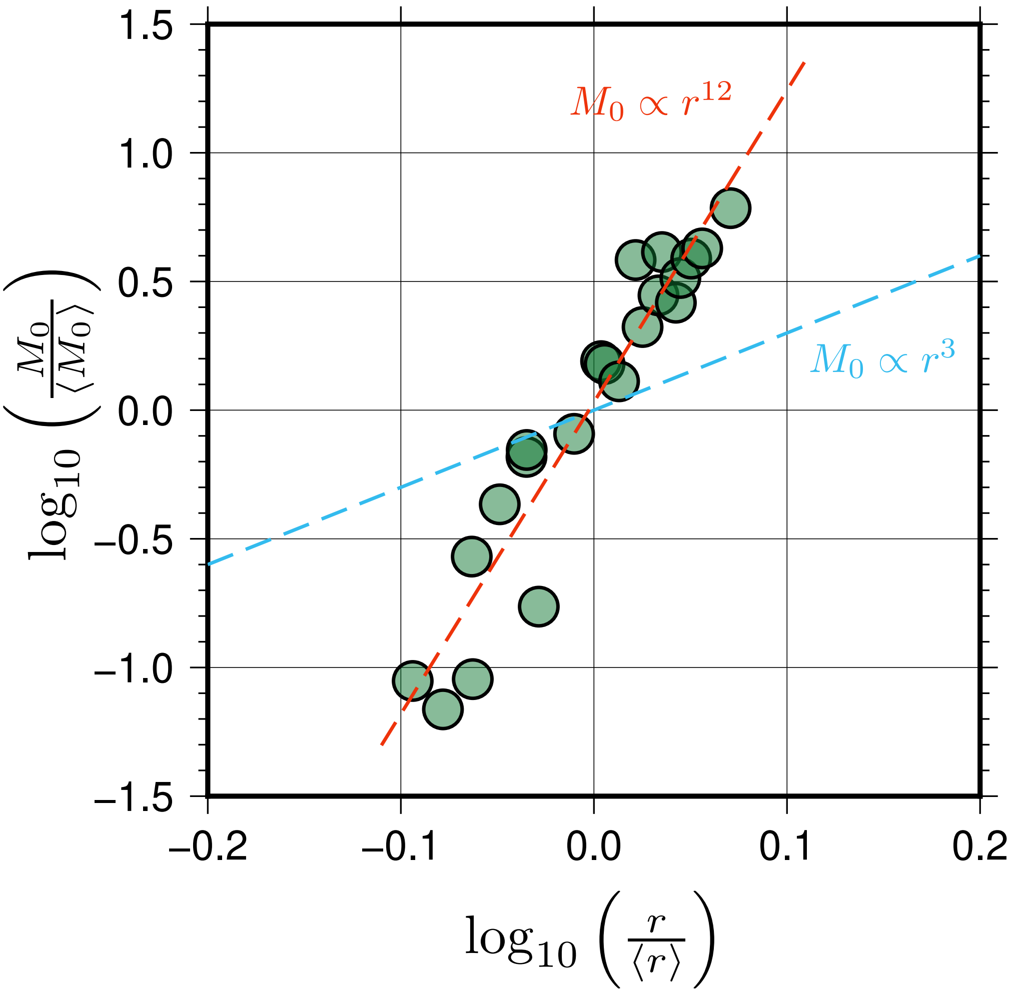

Figure 5. Normalized moment as a function of the normalized rupture length (green dots). This shows the scaling between moment and rupture size within a repeating sequence. The blue dashed line shows the typical $M_0 \propto r^3$ scaling while the red dashed line shows the best fit to the data highlighting a significantly different scaling.

lous scaling for low frequency earthquakes in the Mexican subduction zone with an exponent between 8 and 19 depending on the method used. In the Soulz-sous-Forêts geothermal area, Cauchie et al. (2020) show that the scaling relation within repeating earthquake families exhibit a similar scaling with an exponent close to 20 (see figure 4 for an example). For earthquakes on the San-Andreas fault at Parkfield, Harrington and Brodsky (2009) get an exponent of 17.

All these observations show that for a single family the seismic moment varies at most over 2 orders of magnitude. Our simulation results are in good agreement with these reported observations and thus constitute a possible explanation for this observed anomalous scaling.

The variation of stress drop observed in natural earthquakes and the associated non self-similar scaling could also arise from other considerations. Indeed, as noted by Kaneko and Shearer (2015), rupture directivity or effects of complex geometry compared to the simplistic circular rupture model could also give rise to a variation of the earthquake moment with an almost constant corner frequency. It is also possible, as demonstrated by numerical simulations, that a fault with heterogeneous strength can lead to seismic ruptures on a same fault patch displaying variable moments but nearly constant apparent rupture size (Lin & Lapusta, 2018). Considering the diversity of these effects and their randomness, it seems quite unlikely that they all favorably contribute to produce the anomalous scaling observed across various tectonic settings. We would rather expect that such complexities produce scattering around an average value without any systematic trend. The anomalous scaling inferred from earthquake observations has been also explained by invoking a totally different mechanism involving elastic collisions between fault gouge particles (Tsai & Hirth, 2020).

Our model is limited in several aspects. First, we simulated a 1D fault in a 2D medium; some deviations can arise compared to a rupture on a 2D fault. Our approach also requires some assumptions on the slip distribution in order to compute the potency of each rupture. However, Li et al. (2022) recently show that numerous outcomes of 2D and 3D numerical earthquake cycle models, such as stress drop, are comparable. This supports the validity of the presented results for higher dimension. Secondly, we did not incorporate most recent advances in friction models and fault weakening mechanisms, for instance thermal pressurization or flash weakening processes (Acosta et al., 2018; Lambert et al., 2021). We thus acknowledge that the additional physics contained in these models can give rise to results different than the ones reported here. Furthermore, we did not perform a systematic parametric study, varying the a, b and D_c parameters to test their influence on the resolved scaling. The set of parameters tested in this study has been previously considered in other simulations whose results where found stable while perturbing these values (Chen & Lapusta, 2009). Furthermore, here we only considered an isolated asperity, not interacting with any other asperities. However, faults generally contain several seismic patches that can interact and trigger each other. It remains to be investigated how these interactions can influence the properties derived in this study and impact the observed scaling, Finally, we stress out that the normal stress on an asperity is not-necessarily uniform (Schmittbuhl et al., 2006). This can lead to some important effects as the change of fluid pressure on the fault can lead to change of the contact area of the asperity and thus redistribute stress locally and modify the asperity. Here we preferred to keep a rather simple model which, despite its limitations, offers a straightforward mechanism for interpreting the variation of moment despite similar rupture size observed for numerous repeating earthquake sequences worldwide. Our model proposes that these characteristics can be well understood within the framework of a frictional fault with varying average normal stress. This model requires normal stress fluctuations at the location of the asperity. The most direct explanation for such fluctuations involves the presence of fluid pressure and its variation. The existence of fluid at the location of the seismogenic patch is well understood for geothermal reservoirs but is still debated as a necessary component for the generation of low frequency earthquakes in subduction zones (Saffer & Tobin, 2011). The change of fluid pressure on the fault can then arise from a variation of the fluid pressure from the source region or because slip on a nearby portion of the fault modifies the fluid flow and locally enhances fluid pressure (e.g. Shapiro et al., 2018).

In conclusion our study highlights that a repeating earthquake sequence, at the transition between the seismic and aseismic slip, exhibits a peculiar scaling behavior that can be used as an indicator of proximity to the frictional regime change.

5 Open Research

No data were used in this study. Version 2.3 of the software QDYN used for modeling the seismic cyle is preserved at doi:10.5281/zenodo.322459, available via GNU General Public License v3.0 only and developed openly at https://github.com/ydluo/qdyn.

Acknowledgments
We thank M. Bouchon and J. Elkhoury for discussions about the origin of the unusual scaling.

References

Acosta, M., Passelègue, F., Schubnel, A., & Violay, M. (2018). Dynamic weakening during earthquakes controlled by fluid thermodynamics. *Nature communications*, *9*(1), 1–9.
Ampuero, J.-P., & Rubin, A. M. (2008). Earthquake nucleation on rate and state faults–aging and slip laws. *Journal of Geophysical Research: Solid Earth*, *113*(B1).
Barbot, S. (2019). Slow-slip, slow earthquakes, period-two cycles, full and partial ruptures, and deterministic chaos in a single asperity fault. *Tectonophysics*, *768*, 228171.
Bostock, M. G., Thomas, A. M., Savard, G., Chuang, L., & Rubin, A. M. (2015). Magnitudes and moment-duration scaling of low-frequency earthquakes beneath southern vancouver island. *Journal of Geophysical Research: Solid Earth*, *120*(9), 6329–6350.
Bouchon, M., Karabulut, H., Aktar, M., Özalaybey, S., Schmittbuhl, J., & Bouin, M.-P. (2011). Extended nucleation of the 1999 m w 7.6 izmit earthquake. *science*, *331*(6019), 877–880.
Bourouis, S., & Bernard, P. (2007). Evidence for coupled seismic and aseismic fault slip during water injection in the geothermal site of Soultz (France), and implications for seismogenic transients. *Geophys. J. Int.*, *169*(2), 723–732.
Cauchie, L., Lengliné, O., & Schmittbuhl, J. (2020). Seismic asperity size evolution during fluid injection: case study of the 1993 soultz-sous-forêts injection. *Geophysical Journal International*, *221*(2), 968–980.
Chen, T., & Lapusta, N. (2009). Scaling of small repeating earthquakes explained by interaction of seismic and aseismic slip in a rate and state fault model. *Journal of Geophysical Research: Solid Earth*, *114*(B1).
Cornet, F., Helm, J., Poitrenaud, H., & Etchecopar, A. (1997). Seismic and aseismic slips induced by large-scale fluid injections. *Pure Appl. Geophys.*, *150*, 563–583.
De Barros, L., Cappa, F., Deschamps, A., & Dublanchet, P. (2020). Imbricated aseismic slip and fluid diffusion drive a seismic swarm in the corinth gulf, greece. *Geophysical Research Letters*, *47*(9), e2020GL087142.
De Barros, L., Guglielmi, Y., Rivet, D., Cappa, F., & Duboeuf, L. (2018). Seismicity

and fault aseismic deformation caused by fluid injection in decametric in-situ experiments. *Comptes Rendus Geoscience*, *350*(8), 464–475.

Dieterich, J. H. (1992). Earthquake nucleation on faults with rate-and state-dependent strength. *Tectonophysics*, *211*(1–4), 115 - 134.

Duputel, Z., Tsai, V. C., Rivera, L., & Kanamori, H. (2013). Using centroid time-delays to characterize source durations and identify earthquakes with unique characteristics. *Earth Planet. Sc. Lett.*, *374*, 92–100.

Eshelby, J. D. (1957). The determination of the elastic field of an ellipsoidal inclusion, and related problems. *Proceedings of the royal society of London. Series A. Mathematical and physical sciences*, *241*(1226), 376–396.

Farge, G., Shapiro, N. M., & Frank, W. B. (2020). Moment-duration scaling of low-frequency earthquakes in guerrero, mexico. *Journal of Geophysical Research: Solid Earth*, *125*(8), e2019JB019099.

Frank, W. B., Radiguet, M., Rousset, B., Shapiro, N. M., Husker, A. L., Kostoglodov, V., ... Campillo, M. (2015). Uncovering the geodetic signature of silent slip through repeating earthquakes. *Geophysical Research Letters*, *42*(8), 2774–2779.

Gischig, V. S. (2015). Rupture propagation behavior and the largest possible earthquake induced by fluid injection into deep reservoirs. *Geophysical Research Letters*, *42*(18), 7420–7428.

Harrington, R. M., & Brodsky, E. E. (2009). Source duration scales with magnitude differently for earthquakes on the San Andreas fault and on secondary faults in Parkfield, California. *B. Seismol. Soc. Am.*, *99*(4), 2323–2334.

Kaneko, Y., & Shearer, P. (2015). Variability of seismic source spectra, estimated stress drop, and radiated energy, derived from cohesive-zone models of symmetrical and asymmetrical circular and elliptical ruptures. *Journal of Geophysical Research: Solid Earth*, *120*(2), 1053–1079.

Kato, N. (2012). Dependence of earthquake stress drop on critical slip-weakening distance. *Journal of Geophysical Research: Solid Earth*, *117*(B1).

Lambert, V., Lapusta, N., & Faulkner, D. (2021). Scale dependence of earthquake rupture prestress in models with enhanced weakening: Implications for event statistics and inferences of fault stress. *Journal of Geophysical Research: Solid Earth*, *126*(10), e2021JB021886. doi: https://doi.org/10.1029/2021JB021886

Lapusta, N., & Rice, J. R. (2003). Nucleation and early seismic propagation of small and large events in a crustal earthquake model. *Journal of Geophysical Research: Solid Earth*, *108*(B4).

Lengliné, O., Boubacar, M., & Schmittbuhl, J. (2017). Seismicity related to the hydraulic stimulation of grt1, rittershoffen, france. *Geophysical Journal International*, *208*(3), 1704–1715.

Lengliné, O., Lamourette, L., Vivin, L., Cuenot, N., & Schmittbuhl, J. (2014). Fluid-induced earthquakes with variable stress drop. *Journal of Geophysical Research: Solid Earth*, *119*(12), 8900–8913.

Li, M., Pranger, C., & van Dinther, Y. (2022). Characteristics of earthquake cycles: A cross-dimensional comparison of 0d to 3d numerical models. *Journal of Geophysical Research: Solid Earth*, e2021JB023726.

Lin, Y.-Y., & Lapusta, N. (2018). Microseismicity simulated on asperity-like fault patches: On scaling of seismic moment with duration and seismological estimates of stress drops. *Geophysical Research Letters*, *45*(16), 8145–8155.

Lin, Y.-Y., Ma, K.-F., Kanamori, H., Song, T.-R. A., Lapusta, N., & Tsai, V. C. (2016). Evidence for non-self-similarity of microearthquakes recorded at a taiwan borehole seismometer array. *Geophysical Journal International*, *206*(2), 757–773.

Luo, Y., & Ampuero, J.-P. (2018). Stability of faults with heterogeneous friction properties and effective normal stress. *Tectonophysics*, *733*, 257–272.

Luo, Y., Ampuero, J. P., Galvez, P., van den Ende, M., & Idini, B. (2017, February).

Qdyn: a quasi-dynamic earthquake simulator (v1.1). Zenodo. Retrieved from `https://doi.org/10.5281/zenodo.322459` doi: 10.5281/zenodo.322459

Miller, S. A. (2013). The role of fluids in tectonic and earthquake processes. *Advances in geophysics*, *54*, 1–46.

Passelègue, F. X., Almakari, M., Dublanchet, P., Barras, F., Fortin, J., & Violay, M. (2020). Initial effective stress controls the nature of earthquakes. *Nature communications*, *11*(1), 1–8.

Rubin, A. M. (2008). Episodic slow slip events and rate-and-state friction. *Journal of geophysical research*, *113*(B11).

Rubin, A. M., & Ampuero, J.-P. (2005). Earthquake nucleation on (aging) rate and state faults. *Journal of Geophysical Research: Solid Earth*, *110*(B11).

Saffer, D. M., & Tobin, H. J. (2011). Hydrogeology and mechanics of subduction zone forearcs: Fluid flow and pore pressure. *Annual Review of Earth and Planetary Sciences*, *39*, 157–186.

Savage, J. (1972). Relation of corner frequency to fault dimensions. *Journal of geophysical research*, *77*(20), 3788–3795.

Schmittbuhl, J., Chambon, G., Hansen, A., & Bouchon, M. (2006). Are stress distributions along faults the signature of asperity squeeze? *Geophysical research letters*, *33*(13).

Scholz, C. H. (1998). Earthquakes and friction laws. *Nature*, *391*(6662), 37–42.

Scuderi, M. M., & Collettini, C. (2016). The role of fluid pressure in induced vs. triggered seismicity: Insights from rock deformation experiments on carbonates. *Scientific reports*, *6*, 24852.

Shapiro, N. M., Campillo, M., Kaminski, E., Vilotte, J.-p., & Jaupart, C. (2018). Low-frequency earthquakes and pore pressure transients in subduction zones. *Geophysical Research Letters*, *45*(20), 11–083.

Thomas, M. Y., Lapusta, N., Noda, H., & Avouac, J.-P. (2014). Quasi-dynamic versus fully dynamic simulations of earthquakes and aseismic slip with and without enhanced coseismic weakening. *Journal of Geophysical Research: Solid Earth*, *119*(3), 1986–2004.

Tsai, V. C., & Hirth, G. (2020). Elastic impact consequences for high-frequency earthquake ground motion. *Geophysical Research Letters*, *47*(5), e2019GL086302.

Warren-Smith, E., Fry, B., Wallace, L., Chon, E., Henrys, S., Sheehan, A., … Lebedev, S. (2019). Episodic stress and fluid pressure cycling in subducting oceanic crust during slow slip. *Nature Geoscience*, *12*(6), 475–481.

Supporting Information for "Scaling of repeating earthquakes at the transition from aseismic to seismic slip"

O. Lengliné[1], J.P. Ampuero[2]J. Schmittbuhl[1]

[1]EOST/ITES, Université de Strasbourg/CNRS, UMR7063, 5 rue Ren é Descartes, 67084 Strasbourg Cedex, France

[2]Université Côte d'Azur, IRD, CNRS, Observatoire de la Côte d'Azur, Géoazur, 250 rue Albert Einstein, Sophia Antipolis, 06560 Valbonne, France

Contents of this file

1. Texts S1 and S2
2. Figures S1 and S2
3. Tables S1 and S2

Text S1 - Numerical Modeling Here we document the equations governing the rate-and-state friction model that are used in our analysis and implemented in the QDYN

Corresponding author: O. Lengliné, École et Observatoire des Sicences de la Terre, Université de Strasbourg, 5 rue René Descartes, 67084 Strasbourg, France. (lengline@unistra.fr

software (Luo et al., 2017). In this model the fiction coefficient, μ is

$$\mu = \mu_{ss} + a \ln \left(\frac{v}{v_{ss}} \right) + b \ln \left(\frac{v_{ss}\theta}{D_c} \right), \quad (1)$$

where μ_{ss} is the steady state friction coefficient, at the sliding speed v_{ss}. The parameters a and b are constitutive parameters quantifying the velocity and state effects, respectively. D_c is a critical slip distance and θ is a state variable governs by the ageing law

$$\dot{\theta} = 1 - \frac{v\theta}{D_c}. \quad (2)$$

The realization of the simulation are performed such that everywhere along the fault and at each time step $\tau = \mu\sigma_n$ and

$$\tau(x,t) = \tau_\infty + \frac{G}{2}H(u) - \frac{G}{2C_S}v \quad (3)$$

where $\tau(x,t)$ is the shear stress at position x and time t, τ_∞ is the external shear loading, u and v are respectively the slip and slip speed, G is the shear modulus and C_S is the shear wave speed, imposed here at 3000 m.s^{-1}. The term H is a linear functional representing the static stress transfer due to slip and the third term represents seismic radiation damping to approximate inertial effects by considering the stress reduction due to the radiation of seismic waves.

Text S2 - Simulating a perturbation of normal stress The aim of this supporting information is to document an alternative approach for modeling the variation of normal stress, σ_n imposed to a fault. Here we run simulations for a fault with similar properties as in the manuscript and with $R = 100$ m and $\sigma_n = 50$ MPa. We then imposed a step increase of the normal stress at various times T_i with i varying between 1 to 7. These times sample the whole duration of the seismic cycle of the asperity (See figure S1). We are interested in comparing if the fist seismic rupture that will happened following this increase in normal load is dependent on the time at which this perturbation was imposed. More precisely we want to observe if there are any differences in terms of moment and rupture length between these ruptures and the ruptures generated imposing a constant normal stress of $\sigma_n = 70$ MPa over the whole duration of the simulation.

We report in table S1 the results of our new simulations. We see that the time of the perturbation has insignificant influence on the moment and rupture length of the ensuing rupture. Furthermore we show in Table S2 that the newly simulated ruptures are identical to ruptures modeled in the constant σ_n=70 MPa simulations.

References

Luo, Y., Ampuero, J. P., Galvez, P., van den Ende, M., & Idini, B. (2017, February). *Qdyn: a quasi-dynamic earthquake simulator (v1.1).* Zenodo. Retrieved from `https://doi.org/10.5281/zenodo.322459` doi: 10.5281/zenodo.322459

Table S1. Seismic moment and rupture radius of the first earthquake occurring after perturbing the normal stress from $\sigma_n = 50$ MPa to $\sigma_n = 70$ MPa at different times T_i shown in Figure S1. The resulting radii are identical at the resolution length of the grid discretization, $dx = 1000/1024$ m, while the moment varies only slightly.

Time	Moment, $\log_{10}(M_0/1\ \mathrm{N \cdot m})$	Radius, r (m)
T_1	13.637	110.839
T_2	13.639	110.839
T_3	13.635	110.839
T_4	13.648	110.839
T_5	13.614	110.839
T_6	13.644	110.839
T_7	13.644	110.839

Table S2. Seismic moment and rupture radius obtained in earthquake cycle simulations with constant normal stress on an asperity of size $R = 100$ m. The rupture properties reported in Table S1 are nearly identical to those obtained in seismic cycles with $\sigma_n = 70$ MPa and are significantly different to those observed for $\sigma_n = 50$ MPa

Nomal Stress (MPa)	Moment, $\log_{10}(M_0/1\ \mathrm{N \cdot m})$	Radius, r (m)
50	13.446	105.957
50	13.446	105.957
50	13.446	105.957
50	13.444	105.957
70	13.636	110.839
70	13.636	110.839
70	13.636	110.839

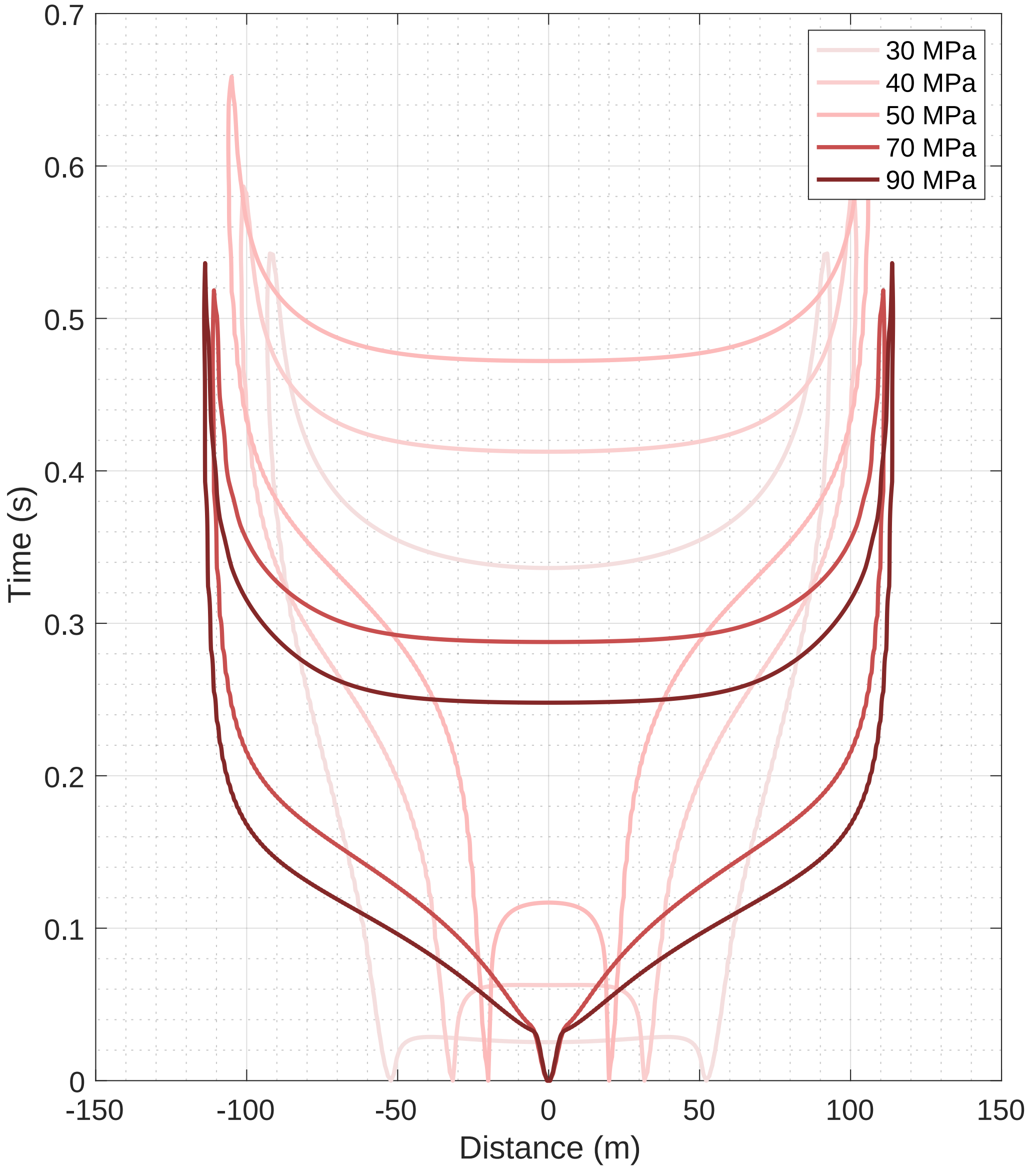

Figure S1. Contours highlighting the slip speed $v(x,t) = v_{th}$ for several values of the normal stress (colored lines). The contours are represented as a function of time, t and distance along fault, x during a simulated earthquake. The time is set here such that t_s=0. The simulation is performed for R=100m.

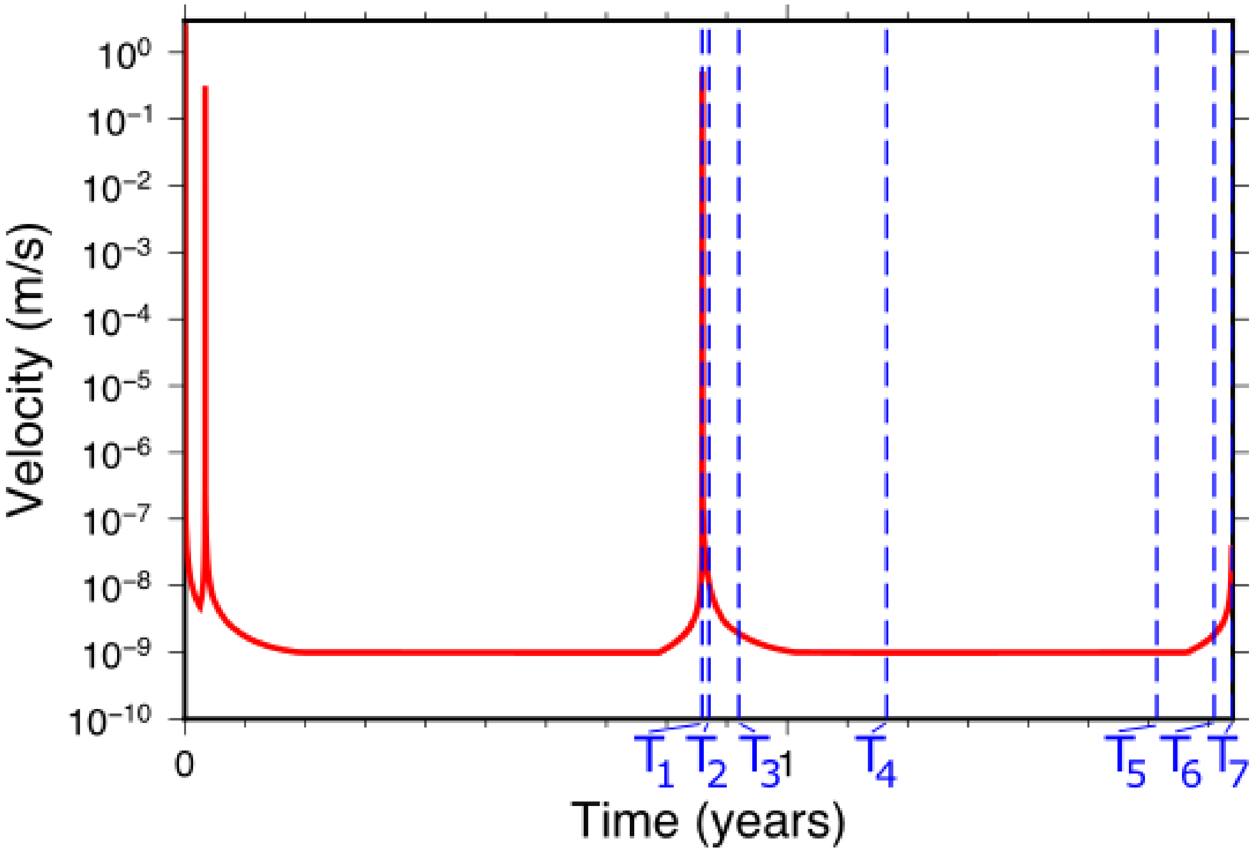

Figure S2. Maximum slip velocity as a function of time for an asperity of size $R = 100$ m and normal stress $\sigma_n = 50$ MPa. After the first two ruptures, affected by the initial conditions, a periodic earthquake cycle is established (see Figure 1). We paused this simulation at several times, T_i, $i \in [1, 7]$, increased the normal stress to $\sigma_n = 70$ MPa, and resumed the simulation. We analyze below how the magnitude and rupture size of the next earthquake following the normal stress increase are affected by the timing of the perturbation, T_i.